© 2021. Published by The Company of Biologists Ltd | Development (2021) 148, dev199453. doi:10.1242/dev.199453

RESEARCH ARTICLE

FOXO1 mediates hypoxia-induced G0/G1 arrest in ovarian somatic granulosa cells by activating the TP53INP1-p53-CDKN1A pathway

Chengyu Li[1], Zhaojun Liu[1], Gang Wu[1], Ziyu Zang[1], Jia-Qing Zhang[2], Xiaoxuan Li[1], Jingli Tao[1], Ming Shen[1,*] and Honglin Liu[1,*]

ABSTRACT

The development of ovarian follicles constitutes the foundation of female reproduction. The proliferation of granulosa cells (GCs) is a basic process required to ensure normal follicular development. However, the mechanisms involved in controlling GC cell cycle are not fully understood. Here, by performing gene expression profiling in the domestic pig (*Sus scrofa*), we showed that cell cycle arrest at G0/G1 phase is highly correlated with pathways associated with hypoxic stress and FOXO signalling. Specifically, the elevated proportion of GCs at the arrested G0/G1 phase was accompanied by increased nuclear translocation of FOXO1 under conditions of hypoxia both *in vivo* and *in vitro*. Furthermore, phosphorylation of 14-3-3 by the JNK kinase is required for hypoxia-mediated FOXO1 activation and the resultant G0/G1 arrest. Notably, a FOXO1 mutant without DNA-binding activity failed to induce G0/G1 arrest of GCs during hypoxia. Importantly, we identified a new target gene of FOXO1, namely *TP53INP1*, which contributes to suppression of the G1-S cell cycle transition in response to hypoxia. Furthermore, we demonstrated that the inhibitory effect of the FOXO1-TP53INP1 axis on the GC cell cycle is mediated through a p53-CDKN1A-dependent mechanism. These findings could provide avenues for the clinical treatment of human infertility caused by impaired follicular development.

KEY WORDS: Cell cycle, G0/G1 arrest, Porcine granulosa cells, Hypoxia, FOXO1-TP53INP1 signalling

INTRODUCTION

Ovarian functions in mammals are mediated through a specialized compartment called the ovarian follicle, comprising a single oocyte surrounded by multiple layers of somatic granulosa cells (GCs). In developing follicles, GCs proliferate rapidly to support follicular growth, maturation and ovulation (Gougeon, 1996). The mitogenic activity of GCs is regulated, at least in part, by hormones secreted from the pituitary and neighbouring cells (Robker and Richards, 1998). In addition, several intraovarian growth factors, such as insulin-like growth factor-I (IGF-I), epidermal growth factor (EGF), transforming growth factor-beta (TGFβ) and fibroblast growth factor (FGF), can affect GC proliferation (Vanderhyden et al., 1992). Although significant progress has been made in recent years, the mechanisms involved in controlling the GC cell cycle are not fully understood.

The ovarian follicular vascular system directly supplies the nutrition, oxygen and hormones that are required for follicle development (Brown and Russell, 2014). However, angiogenesis is confined to the theca cells outside the basement membrane, a physical barrier that blocks the capillary network from penetrating into the interior of the follicle, thus inhibiting the transport of O_2 to the GC layer. During follicular development, the proliferation of GCs and thickening of the GC compartment further increases the distance from GCs to the follicular vasculature, leading to a progressively deficient supply of O_2 (Bianco et al., 2005; Redmer and Reynolds, 1996; Suzuki et al., 1998). Therefore, it is commonly accepted that GCs exist in a hypoxic environment within ovarian follicles (Nishimura and Okuda, 2015).

In recent years, evidence has accumulated that cells can respond to varying O_2 levels by altering their rates of proliferation (Ortmann et al., 2014). In fact, many different cell types display cell cycle arrest and proliferative retardation during hypoxia (Ortmann et al., 2014). Conversely, rapid proliferation of cells accelerates O_2 consumption, leading to a reduction in cellular O_2 tension (Ortmann et al., 2014). Indeed, regular follicular development is accompanied by a high proliferation rate of GCs. However, Zhang et al. (2018), reported that the expression of some mitosis-related genes in GCs tends to decrease with follicular growth, implicating a possible reduction of GC proliferation activity during folliculogenesis. Interestingly, transcriptome sequencing in porcine large antral follicles revealed gene pathways associated with hypoxia (Munakata et al., 2016). Moreover, our earlier study showed that cobalt chloride ($CoCl_2$), a hypoxia-mimicking agent, could inhibit cell cycle progression in cultured GCs (Li et al., 2020). This prompted us to investigate whether hypoxia is actually involved in the regulation of the cell cycle in ovarian GCs during folliculogenesis.

Cellular proliferation is controlled by molecules that positively or negatively affect transitions through the checkpoints of the cell cycle. Briefly, entry into the cell cycle is positively regulated by a family of protein kinases referred to as cyclin-dependent kinases (CDKs) (Ortmann et al., 2014). By contrast, CDK inhibitors (CKIs) are negative regulators that hinder the cell cycle progression. CKIs, such as CDKN1A (cyclin-dependent kinase inhibitor 1A), function by binding to CDKs and inhibiting their interaction with cyclins, resulting in cellular growth arrest (Ortmann et al., 2014). The expression of CDKN1A is mainly controlled at the transcriptional level by the transcription factor p53 (Li et al., 1994). On activation by p53 during a variety of stresses, CDKN1A directly inhibits the formation of cyclin E-CDK2 complexes, leading to p53-mediated

[1]College of Animal Science and Technology, Nanjing Agricultural University, Nanjing 210095, China. [2]Institute of Animal Husbandry and Veterinary Science, Henan Academy of Agricultural Sciences, Zhengzhou, 450002, China.

*Authors for correspondence (shenm2015@njau.edu.cn; liuhonglin@njau.edu.cn)

C.L., 0000-0001-5361-4442; M.S., 0000-0003-1219-225X; H.L., 0000-0002-7613-4983

Handling Editor: Haruhiko Koseki
Received 21 January 2021; Accepted 13 June 2021

Development (2021) 148, dev199453. doi:10.1242/dev.199453

G1-stage cell cycle arrest (Harper et al., 1995). As one type of stress, hypoxia has been suggested to induce cell cycle arrest at G0/G1 phase and to block G1-to-S transition (Gardner et al., 2001). According to our previous studies, chemical-simulated hypoxia in primary cultured GCs could arrest cells at the G1/S boundary (Li et al., 2020). However, current evidence does not indicate whether and how real hypoxia acts on regulating GC cell cycle *in vivo*.

Here, using high-throughput sequencing technology, we demonstrated hypoxia as a primary component within developing porcine follicles that prevents cell cycle progression of GCs. Our findings suggest an inhibitory role for hypoxia in regulating the G1-S transition by activating the JNK-14-3-3-FOXO1-TP53INP1-p53-CDKN1A signalling axis in ovarian GCs.

RESULTS

Cell cycle progression of ovarian GCs might be regulated by hypoxia and the FOXO1 signalling pathway

Using flow cytometry, we determined the cell cycle distribution of GCs collected from porcine ovarian antral follicles. As shown in Fig. 1A-C, the proportion of GCs at G0/G1 phase tended to increase, whereas the S-and-G2/M phase population decreased with the growing sizes of the follicles, indicating an impaired GC proliferation activity during follicular development. Because follicular growth is supposed to cause hypoxia in GCs (Bianco et al., 2005; Redmer and Reynolds, 1996; Suzuki et al., 1998), it raises the possibility that hypoxia might influence GC proliferation. Interestingly, individual follicles of the same diameter also showed large variations in G0/G1 distribution of GCs (Fig. 1A-D). To investigate whether hypoxia or other factors might contribute to GC cell cycle asynchrony among similar-sized follicles, GCs retrieved from developing follicles around 4 mm in diameter were classified into groups with high G0/G1 distribution (high groups) and low G0/G1 distribution (low groups), which were then subjected to transcriptomic profiling by RNA sequencing (RNA-seq). We found that the transcriptome of the high groups was significantly different from that of the low groups by showing that 638 transcripts were downregulated and 686 transcripts were upregulated in the former (Fig. 1E,F). The expression of ten randomly selected transcripts were verified using quantitative RT-PCR (qRT-PCR), indicating the reliability of the RNA-seq data (Fig. S1). Gene ontology (GO) annotation was performed to assign a functional classification to these differentially expressed genes (DEGs). The top 15 significantly enriched GO terms of the DEGs for each category are shown in Fig. 1G,H. For downregulated biological processes, the DEGs were mainly assigned to cell cycle-related functions (Fig. 1G), implicating that our sampling procedures were specific. Notably, response to hypoxia was enriched at the top list for the upregulated biological process (Fig. 1H), consistent with our above-mentioned speculation regarding the effects of hypoxia on GCs cell cycle. To explore the biochemical pathways further, all DEGs were mapped to terms in the Kyoto Encyclopedia of Genes and Genomes (KEGG) database (https://www.kegg.jp; Fig. 1I). Among the top 20 enriched pathways, we paid greater attention to FOXO1 signalling, because our previous studies suggested FOXO1 to be a crucial mediator of the stress response in ovarian GCs (Li et al., 2020; Shen et al., 2018, 2017, 2012, 2014), and FOXO1 is the only FOXO family member present in our transcriptomic data.

To validate the possible involvement of hypoxia and FOXO1 in modulating GC cell cycle, experiments were performed in porcine ovarian GCs harvested from growing follicles at various stages, including small antral follicles (1-3 mm), medium antral follicles (3-5 mm) and large antral follicles (≥5 mm). As a transcription factor, FOXO1 functions by entering the cell nucleus (Shen et al., 2012). For medium and large antral follicles, increased nuclear distribution of FOXO1 was observed in those with a higher prevalence of GCs in G0/G1 phase (Fig. S2F,K). Linear regression analysis showed that the fraction of the population arrested at G0/G1 was positively correlated with FOXO1 expression in the nuclei (Fig. S2G,L). To test whether hypoxia might be relevant to regulation of the GC cell cycle *in vivo*, the protein level of hypoxia inducible factor-1alpha (HIF-1α), a key endogenous marker of hypoxia, was determined in ovarian GCs. As shown in Fig. S2H,I,M,N, elevated proportions of GCs at G0/G1 correlated strongly with a progressively more hypoxic status as reflected by the accumulation of cellular HIF-1α. Moreover, a significant positive correlation was determined between nuclear distribution of FOXO1 and HIF-1α accumulation in ovarian GCs as mentioned above (Fig. S2J,O). However, no significant correlation was detected among intranuclear FOXO1 protein levels, HIF-1α abundance, and cell cycle distribution in GCs collected from small antral follicles (Fig. S2A-E). Therefore, our *in vivo* findings indicate a potential interaction between hypoxia and FOXO1 signalling in controlling the cell cycle transition of GCs in medium and large antral follicles.

Hypoxia-induced nuclear translocation of FOXO1 causes G0/G1 arrest in cultured GCs

To clarify further the relationship between hypoxia and GC cell cycle without interference from other follicular factors, we applied hypoxia treatment to primary cultured GCs harvested from porcine antral follicles. As shown in Fig. 2A,B, hypoxia significantly increased the percentage of cells in G0/G1 phases, but reduced the fraction in S phase, implicating an inhibitory effect of hypoxia on G1-to-S transition in GCs. To assess whether FOXO1 might be involved in this process, we measured the subcellular localization of FOXO1 in hypoxia-treated GCs. As shown in Fig. 2C,D, hypoxia facilitated nuclear translocation of FOXO1, as suggested by the increased percentage of cells with FOXO1 in the nucleus. To examine whether FOXO1 might be required for hypoxia-mediated G0/G1 cell cycle arrest, we blocked FOXO1 expression using RNA interference. Six siRNAs against *FOXO1* were first screened for their potency and specificity. Two out of these candidates were identified as the most potent and specific siRNAs in silencing *FOXO1* and were used for subsequent experiments (Fig. S3A). As shown in Fig. 2E,F, knocking down *FOXO1* expression markedly restored the proportion of GCs in the S-phase population by driving cells out of the G0/G1 phase. Collectively, these data suggest that FOXO1 plays a pivotal role in the hypoxia-induced G0/G1 arrest of GCs.

JNK-mediated dissociation of FOXO1 from 14-3-3 promotes FOXO1 nuclear translocation upon hypoxic stimulation

Among the stress-responsive kinases, SAPK/JNK, p44/42 MAPK and p38 MAPK are known to target FOXOs and regulate their activity through a cytoplasmic-nuclear shuttling mode (Klotz et al., 2015). To explore further the mechanism of FOXO1 regulation under hypoxia, we examined whether these pathways would affect FOXO1 localization and cell cycle progression in primary cultured GCs. As shown in Fig. 3A-C and Fig. S4A-C, unregulated JNK activity, as reflected by elevated phosphorylation status at Thr183/Tyr185, correlated strongly with the increased nuclear distribution of FOXO1 in GCs with prolonged hypoxic treatment (Pearson correlation test; $P<0.01$). However, p44/42 MAPK and p38 MAPK presented no evident response to hypoxia. We also determined the possible involvement of AKT, a major upstream suppressor of

Development (2021) 148, dev199453. doi:10.1242/dev.199453

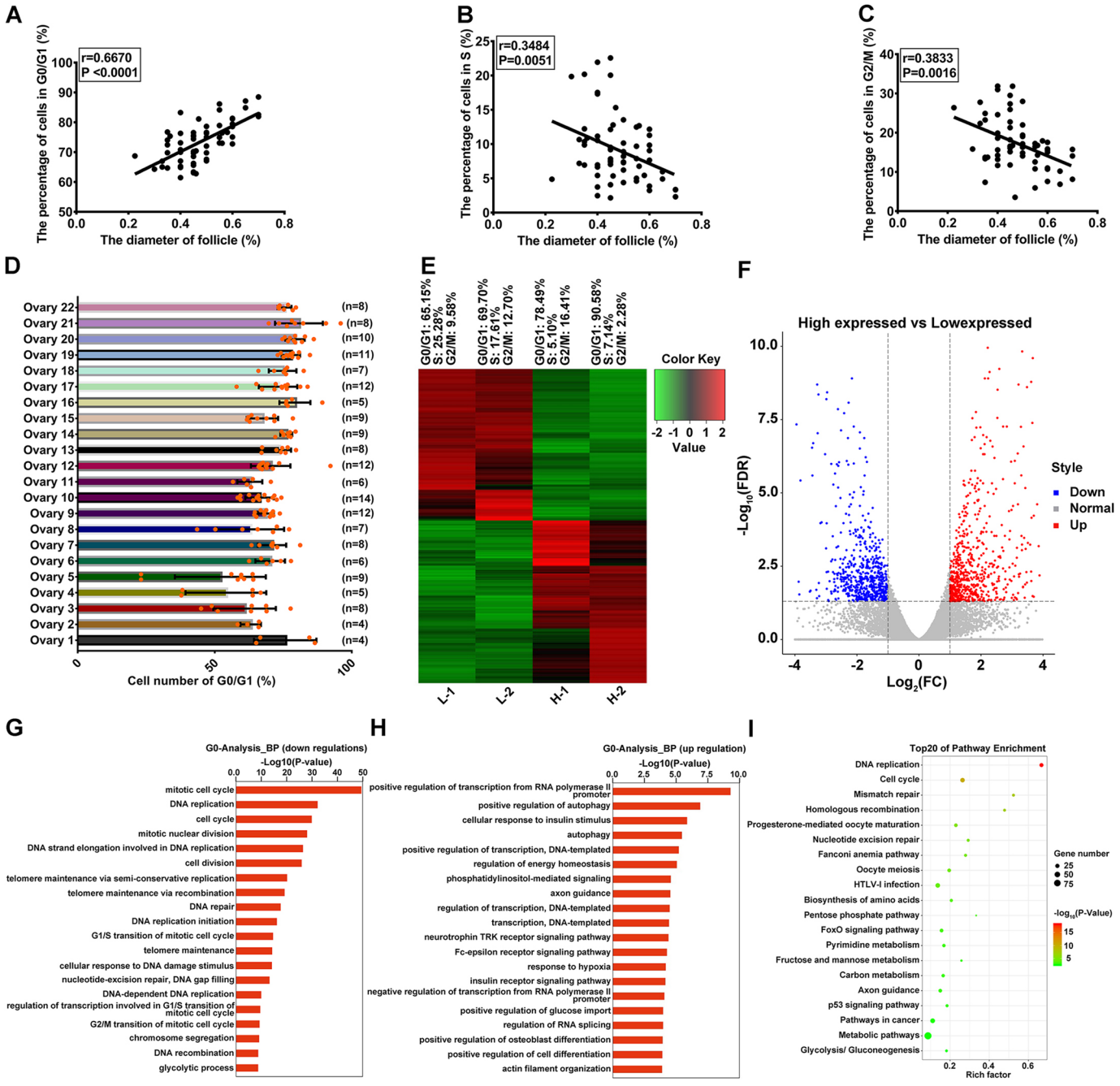

Fig. 1. Transcriptomic profiling of ovarian GCs with high G0/G1 distribution (high groups) and low G0/G1 distribution (low groups). (A-C) GCs in porcine antral follicles were isolated for flow cytometric detection of cell cycle. The relationship between follicular size and GC cell cycle was analysed by linear regression in 70 follicles. (D,E) Ovarian follicles (around 4 mm in diameter) dissected from each of 22 ovaries were individually torn apart to isolate GCs, which were then subjected to cell cycle determination with flow cytometry. The bar chart shows the G0/G1 distribution of GCs in follicles obtained from ovaries as indicated (D). Each dot represents a follicle. Based on the ratio of cells in G0/G1 phase, GCs were classified into four groups with two high G0/G1 distribution groups (high groups) and two low G0/G1 distribution groups (low groups), both of which were processed for RNA-seq analysis. The heat map shows differentially expressed transcripts in GCs from high groups (H-1, H-2) and low groups (L-1, L-2) (E). (F) A volcano plot depicting up- (red) and downregulated (blue) genes identified in RNA-seq in high groups compared with low groups. (G,H) Biological implications based on functional annotation gene clustering. Significantly enriched downregulated (G) and upregulated (H) biological processes (P<0.05) between high groups versus low groups were identified by Fisher's exact test. (I) The top 20 KEGG enrichment pathways for differentially expressed transcripts between the high and low groups. Fisher's exact test was applied to identify statistically significant pathways (P<0.05) associated with differentially expressed transcripts.

FOXO1 activity (Klotz et al., 2015). Paradoxically, the active form of AKT, namely p-AKT (phosphorylated at Ser473), showed elevated expression during hypoxic exposure (Fig. 3A), suggesting that AKT might be irrelevant to hypoxia-mediated FOXO1 activation in GCs. To verify the impact of JNK on FOXO1 subcellular localization, we blocked JNK activity using the inhibitor SP600125. Immunofluorescence staining indicated that the nuclear translocation of FOXO1 upon hypoxia stimulation was inhibited after SP600125 treatment (Fig. 3D,E). Consistent with this, in GCs subjected to hypoxia the JNK inhibitor significantly increased

Development (2021) 148, dev199453. doi:10.1242/dev.199453

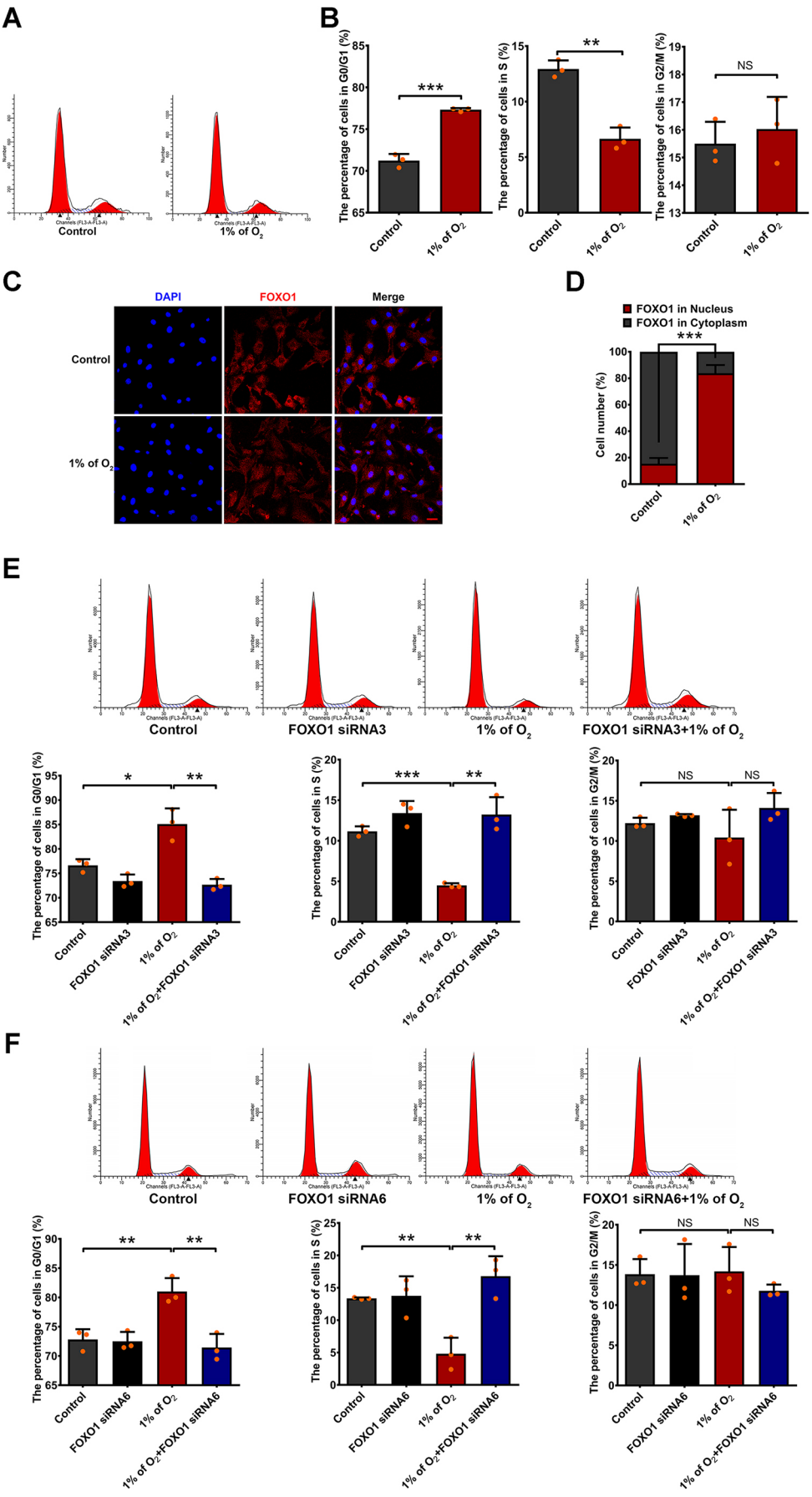

Fig. 2. Hypoxia-induced nuclear translocation of FOXO1 arrests GCs at G0/G1 phase. (A) GCs were cultured under normoxia (20% O_2; control) or hypoxia (1% O_2) for 24 h, and then collected for cell cycle analysis using flow cytometry. (B) The percentage of GCs in G0/G1, S or G2/M phase was quantified using the ModFit LT 3.2 program. (C) GCs incubated in 20% O_2 (control) or 1% O_2 for 12 h were collected to observe the subcellular localization of FOXO1 by immunofluorescence. Scale bar: 20 µm. (D) The percentage of GCs with FOXO1 in the nucleus (red bars) and in the cytoplasm (grey bars). Experiments were performed in triplicate, and cells were counted in three randomly selected fields in each coverslip. (E,F) GCs transfected with FOXO1 siRNAs (siRNA3, siRNA6) or scramble control siRNA for 12 h were cultured for an additional 24 h under normoxia (20% O_2) or hypoxia (1% O_2), and then collected for cell cycle analysis using flow cytometry. The cell cycle distribution of GCs was quantified using ModFit LT 3.2 software. Data are represented as mean ±s.e.m.; n=3. *P<0.05, **P<0.01, ***P<0.001; NS, not significant (P>0.05).

Development (2021) 148, dev199453. doi:10.1242/dev.199453

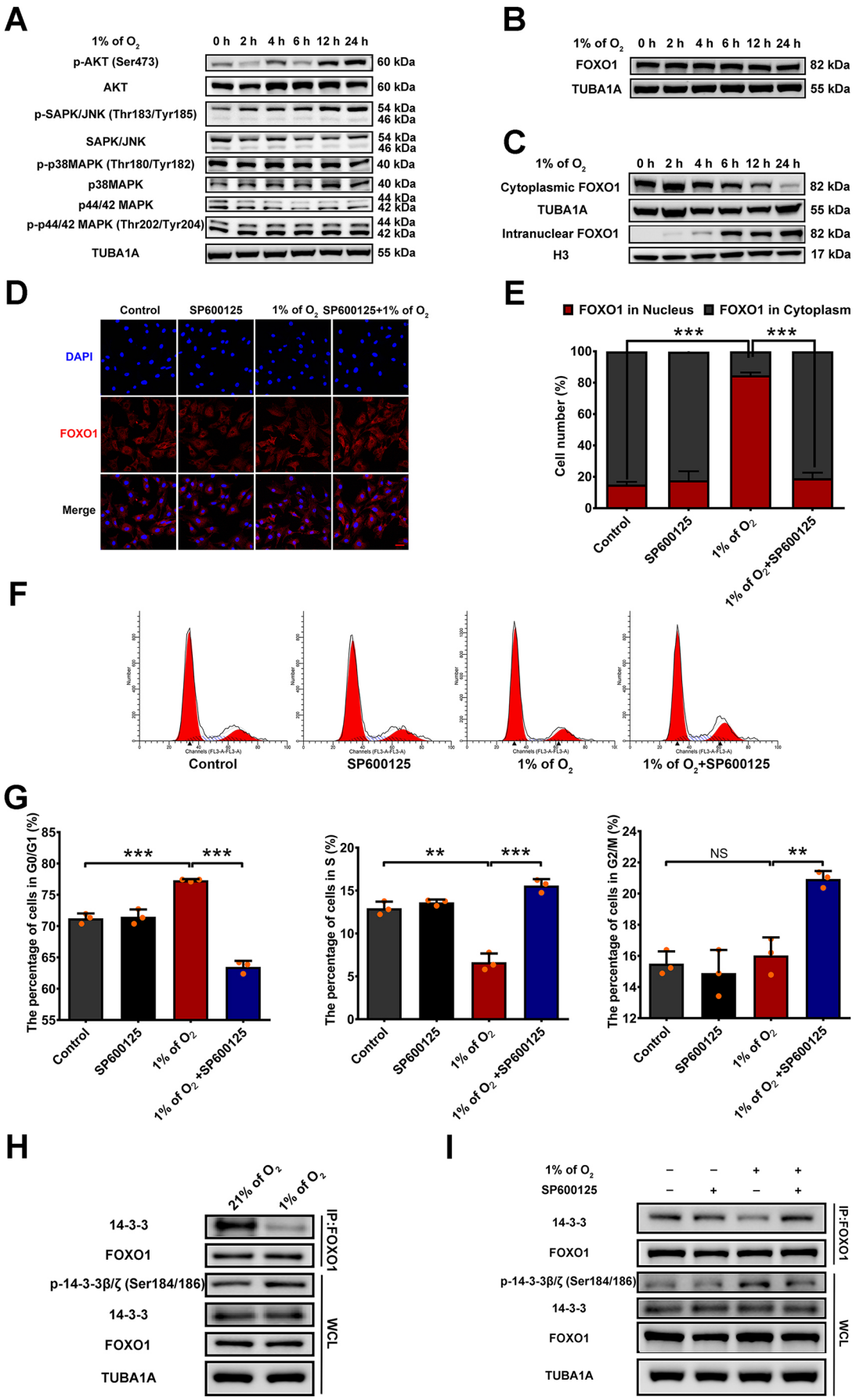

Fig. 3. See next page for legend.

Development (2021) 148, dev199453. doi:10.1242/dev.199453

Fig. 3. Nuclear localization of FOXO1 is mediated through the JNK-14-3-3 pathway in hypoxic GCs. (A,B) GCs exposed to 1% O_2 for 0, 2, 4, 6, 12 or 24 h were retrieved for immunoblotting analysis of signalling proteins (A) or FOXO1 expression (B) as indicated. (C) GCs incubated with 1% O_2 for 0, 2, 4, 6, 12 or 24 h were lysed for the separation of nuclear and cytosolic proteins. FOXO1 in the nucleus and the cytoplasm was detected using western blotting. Histone H3 and TUBA1A served as loading controls for nuclear and cytoplasmic proteins, respectively. (D) GCs were cultured in medium containing 10 µM SP600125 for 2 h, exposed to 1% O_2 for 12 h, and then collected to observe the subcellular localization of FOXO1 by immunofluorescence. (E) Percentage of cells with FOXO1 in the nucleus (red bars) and in the cytosol (grey bars) (quantitative analysis of data in D). (F,G) GCs pretreated with JNK inhibitor (10 µM SP600125 for 2 h) and cultured under hypoxia (1% O_2) for 24 h were collected for cell cycle analysis using flow cytometry (F). The cell cycle distribution of GCs was quantified using ModFit LT 3.2 software (G). (H,I) GCs untreated (H,I) or pretreated with 10 µM SP600125 for 2 h (I) were cultured under normoxia (20% O_2) or hypoxia (1% O_2) for 12 h, and then processed for immunoprecipitation assay to determine the interaction of 14-3-3 and FOXO1 using the antibodies as indicated. Data are represented as mean±s.e.m.; n=3. **P<0.01, ***P<0.001; NS, not significant (P>0.05).

the proportion of cells in S phase, but reduced the population in G0/G1 phases, implicating a recovery of the G1-to-S transition (Fig. 3F,G).

JNK has been documented to induce the phosphorylation of 14-3-3β and ζ at Ser186 and 184, respectively, thereby preventing the association of 14-3-3 with its target proteins (Sunayama et al., 2005). As the formation of the FOXO1-14-3-3 complex is required for the cytoplasmic transport of FOXO1 in mammalian cells (Huang and Tindall, 2007), we wondered whether hypoxia-induced activation of JNK would affect the binding between 14-3-3 and FOXO1. To test this assumption, GCs exposed to hypoxia were harvested for immunoprecipitation with an antibody against FOXO1. As shown in Fig. 3H and Fig. S4D, 14-3-3 was co-precipitated by the FOXO1 antibody. The binding affinity of 14-3-3 to FOXO1 was remarkably decreased after incubation with 1% O_2, along with an elevated level of phosphorylated 14-3-3 under hypoxic conditions. In addition, blocking of JNK activity augmented hypoxia-induced phosphorylation of 14-3-3, followed by a restored association between 14-3-3 and FOXO1 in hypoxic GCs (Fig. 3I, Fig. S4E). Thus, we conclude that dissociation of the FOXO1-14-3-3 complex caused by 14-3-3 phosphorylation through the JNK pathway might be an essential step in hypoxia-mediated suppression of the G1-S transition in ovarian GCs.

A FOXO1 mutant variant lacking DNA-binding activity fails to inhibit the G1-S transition in GCs

Growing evidence indicates that FOXOs can regulate transcription directly through consensus-binding motifs or indirectly via partner proteins (Huang and Tindall, 2007; Ramaswamy et al., 2002). To investigate further how FOXO1 functions in the nucleus, GCs cultured under hypoxia were transfected with vectors encoding FOXO1, including wild-type (WT) FOXO1 (FOXO1-WT) and FOXO1-DBD/FOXO1^{N208A,H212R} (containing two point mutations in the DNA-binding domain), after knocking down endogenous FOXO1 (Fig. S5A). Western blot analysis demonstrated a marked increase in FOXO1 levels in GCs with enforced expression of FOXO1 (Fig. S5A). RNA interference showed no apparent influence on the expression of Flag-tagged FOXO1 detected in both the FOXO1-WT and FOXO1-DBD groups, enabling us to specify the effects of exogenous FOXO1 (Fig. S5A). By performing flow cytometric assay, we found that overexpression of FOXO1-WT restored hypoxia-induced G0/G1 arrest in GCs pretreated with FOXO1 siRNA (Fig. S5B,C). By contrast, the FOXO1-DBD mutant showed no evident effects on this process (Fig. S5B,C). These results suggest that binding to the recognition motifs in target genes might be required for FOXO1-induced G0/G1 arrest in GCs exposed to hypoxia.

FOXO1 influences the expression of genes related to G1-S cell cycle progression in hypoxic GCs

To identify the downstream effectors of FOXO1 signalling, we blocked FOXO1 activity using RNAi, and then determined the expression of checkpoint factors required for G1-S progression in hypoxia-treated GCs. qRT-PCR assay revealed that, among the tested transcripts, the expression patterns of *TP53INP1* and *CDKN1A* were significantly correlated with that of *FOXO1* (P<0.01) in response to hypoxia and FOXO1 siRNA treatment (Fig. S6A). Consistent results were obtained by western blot analysis (Fig. S6B). As shown in Fig. S6B, knockdown of FOXO1 abrogated hypoxia-upregulated expression of TP53INP1 and CDKN1A. In contrast, the protein levels of TP53INP1 and CDKN1A inhibited by *FOXO1* silencing were restored after overexpression of FOXO1-WT, whereas the DBD mutant had no effect (Fig. S6C). These data thus suggest *TP53INP1* and *CDKN1A* as potential downstream target genes of FOXO1 in regulating GC cell cycle during hypoxia exposure.

FOXO1-mediated transcriptional activation of *TP53INP1* prevents the G1-S transition in hypoxic GCs

In fact, the above-mentioned results of CDKN1A expression in hypoxia-treated GCs are expected, as *CDKN1A* has been well described as a transcriptional target of FOXOs (Huang and Tindall, 2007). Compared with *CDKN1A*, there is little evidence regarding whether and how FOXO1 could directly regulate TP53INP1 expression. However, our RNA-seq data indicated *TP53INP1* as a significantly upregulated DEG in ovarian GCs with high G0/G1 distribution (Table 1, Table S5), consistent with the qRT-PCR results as shown in Fig. S6. To test whether FOXO1 would directly activate the expression of *TP53INP1* at the promoter level, a 2072-bp fragment of the *TP53INP1* 5′ untranslated region (UTR) containing the putative FOXO-recognized element (FRE) site or mutated FRE sites was cloned upstream of a luciferase reporter gene as pGL3-TP53INP1 (WT), pGL3-TP53INP1 (M1), pGL3-TP53INP1 (M2) and pGL3-TP53INP1 (M3), respectively (Fig. 4A). These constructs were then co-transfected with pRL-TK and pCMV5-FLAG-FOXO1 (FOXO1-WT) or the control pCMV5 into GCs. As shown in Fig. 4B, enforced expression of the FOXO1-WT vector significantly increased *TP53INP1* promoter activity. In contrast, FRE site mutations markedly reduced the responsiveness of the luciferase reporter to FOXO1 overexpression (Fig. 4B). To confirm whether FOXO1 binds to *TP53INP1* promoter, we next performed chromatin immunoprecipitation (ChIP) assays. GC chromatin was first digested into fragments of 250-700 bp with micrococcal nuclease (Fig. S7) and then used for ChIP experiments. As shown in Fig. 4C-E, the FOXO1 antibody precipitated the *TP53INP1* promoter region around the FRE site. Notably, the signals were significantly enhanced in GCs with hypoxia exposure. Therefore, these data suggest that FOXO1 was recruited directly to the *TP53INP1* promoter for its transcriptional activation in GCs upon exposure to hypoxia.

To test whether TP53INP1 is required for FOXO1-mediated G0/G1 arrest, we transfected GCs with siRNAs against *FOXO1* and/or *TP53INP1* (Fig. S3B). As shown in Fig. 4F,G, blocking the expression of *FOXO1* and *TP53INP1* both facilitated the

Development (2021) 148, dev199453. doi:10.1242/dev.199453

Table 1. TP53INP1 GO terms

GO ID	GO term	*P*-value	FDR	Enrichment
GO:0010508	Positive regulation of autophagy	1.27256E−07	0.000164033	10.02163624
GO:0006914	Autophagy	3.51251E−06	0.002263816	4.09976028
GO:0045893	Positive regulation of transcription, DNA-templated	6.15045E−06	0.003171173	2.171989603
GO:0006355	Regulation of transcription, DNA-templated	3.21588E−05	0.009211701	1.488515336
GO:0006351	Transcription, DNA-templated	3.6158E−05	0.009321529	1.513448459
GO:0008285	Negative regulation of cell proliferation	0.000139139	0.015994479	2.170461325
GO:0007050	Cell cycle arrest	0.000237491	0.021112143	3.006490872
GO:0043065	Positive regulation of apoptotic process	0.000331472	0.025479167	2.257433419
GO:0000045	Autophagic vacuole assembly	0.012311408	0.177848907	3.5791558
GO:0071447	Cellular response to hydroperoxide	0.015152458	0.18553605	10.02163624
GO:0006950	Response to stress	0.01940627	0.18553605	3.198394545
GO:0010506	Regulation of autophagy	0.030735701	0.18553605	3.340545414
GO:0072703	Cellular response to methyl methanesulphonate	0.033261368	0.18553605	30.06490872
GO:0071361	Cellular response to ethanol	0.034041331	0.18553605	6.681090827
GO:0006915	Apoptotic process	0.035437858	0.190728177	1.40574988

passage from G1 to S phase in hypoxic GCs, but FOXO1 siRNA failed to further promote G1-S transition when *TP53INP1* was transcriptionally silenced. In addition, hypoxia-induced CDKN1A expression was remarkably reduced after knocking down the expressions of *FOXO1* and/or *TP53INP1* (Fig. 4H, Fig. S8). Thus, these data confirm that FOXO1 induces *TP53INP1*-dependent G0/G1 arrest in hypoxic GCs.

TP53INP1 acts through p53-CDKN1A signalling to induce G0/G1 arrest during hypoxia

We next sought to identify the downstream effectors of TP53INP1-triggered G0/G1 arrest. The results presented in Fig. 4 indicated that TP53INP1 might be required for hypoxia-induced CDKN1A expression in GCs. Indeed, it has been well documented that CDKN1A is also transcriptionally regulated by p53 (Li et al., 1994). Of note, the KEGG analysis in Fig. 1H revealed p53 signalling to be one of the top 20 enriched pathways in ovarian GCs with high G0/G1 rates. This prompted us to test whether p53 might exert any effects on hypoxia-induced G0/G1 arrest of GCs. As shown in Fig. 5A and Fig. S9A, the increased level of CDKN1A during hypoxia was accompanied by an evident upregulation of p53 expression. To test whether p53 might be required for hypoxia-induced CDKN1A expression, GCs were treated with pifithrin-α, an inhibitor that blocks the transcription activity of p53. The results in Fig. 5B and Fig. S9B showed that the hypoxia-triggered expression of CDKN1A was significantly decreased in GCs treated with the p53 inhibitor. Interestingly, pifithrin-α treatment also inhibited TP53INP1 expression upon hypoxia stimulation. To clarify the relationship among p53, TP53INP1 and CDKN1A, we silenced TP53INP1 activity using RNAi, and then determined the expression of p53 and CDKN1A. As shown in Fig. 5C, Fig. S9C and Fig. 4F, blocking TP53INP1 markedly reduced the protein level of CDKN1A, but had little effect on p53 expression during hypoxia exposure. Therefore, these data indicate the presence of a p53-TP53INP1-CDKN1A axis in hypoxic GCs.

We then examined whether TP53INP1 might contribute to p53-mediated transcriptional activation of CDKN1A. By performing ChIP assay, we observed that the anti-p53 antibody bound to the consensus motif of the p53 binding site located within the *CDKN1A* promoter (Fig. 5D). Notably, knocking down the expression of TP53INP1 abolished the interaction between p53 and the *CDKN1A* promoter in hypoxia-exposed GCs (Fig. 5D-F). In accordance with this, inhibitors or siRNAs against *p53* and *TP53INP1* revealed the approximate level of suppression of CDKN1A expression (Fig. S10), thus suggesting TP53INP1 to be a crucial activator of p53 transcriptional function in hypoxic GCs.

We also determined whether the p53-CDKN1A axis might affect cell cycle progression of GCs exposed to hypoxia. Flow cytometric analysis showed that inhibition of p53 and CDKN1A both markedly restored the proportion of GCs in S phase by driving cells out of G0/G1 phase (Fig. 5G,H, Fig. S3C). Taken together, these data suggest that activation of the p53-CDKN1A axis by TP53INP1 might constitute a primary suppressive mechanism responsible for hypoxia-mediated G0/G1 arrest in GCs.

In vivo validation of mechanisms for G0/G1 arrest in ovarian follicular GCs

To test whether our model of cell cycle regulation would be applicable *in vivo*, GCs collected from developing follicles around 4 mm in diameter were classified into groups with a high G0/G1 distribution (high groups) or a low G0/G1 distribution (low groups). As expected, elevated JNK activity was associated with a more hypoxic status as reflected by the accumulation of HIF-1α in GCs with higher G0/G1 distribution (Fig. 6A, Fig. S11A). In addition, JNK activity was proportional to the intranuclear level of FOXO1, both of which were increased in the high groups (Fig. 6B, Fig. S11B). Moreover, GCs with higher G0/G1 distribution showed upregulated level of phosphorylated 14-3-3, along with an impaired binding affinity of 14-3-3 to FOXO1 (Fig. 6C). Of note, compared with the low groups, the JNK activity, 14-3-3 phosphorylation, and the binding status between 14-3-3 and FOXO1 showed similar trends of change in the high groups (Fig. S11C). These findings suggest the possible involvement of JNK-14-3-3-FOXO1 signalling in controlling GC proliferation under hypoxia *in vivo*.

We next determined the downstream effectors of FOXO1. As shown in Fig. 6D and Fig. S11D, the high groups of GCs showed increased TP53INP1 expression, accompanied by an elevated level of intranuclear FOXO1. Using ChIP-qPCR assays, we further observed increased binding of FOXO1 to the promoter of *TP53INP1* in the high groups (Fig. 6E, Fig. S11E). Concomitantly, the expression of TP53INP1 was proportional to that of CDKN1A in the above-mentioned GC groups (Fig. 6F, Fig. S11F). Further investigation revealed that the upregulated expression of CDKN1A was accompanied by an enrichment of p53 at the promoter region of *CDKN1A* (Fig. 6G, Fig. S11G). Furthermore, TP53INP1 expression was proportional to the p53 binding level at the *CDKN1A* promoter (Fig. S11H). Using histological sections of porcine ovaries, we

Development (2021) 148, dev199453. doi:10.1242/dev.199453

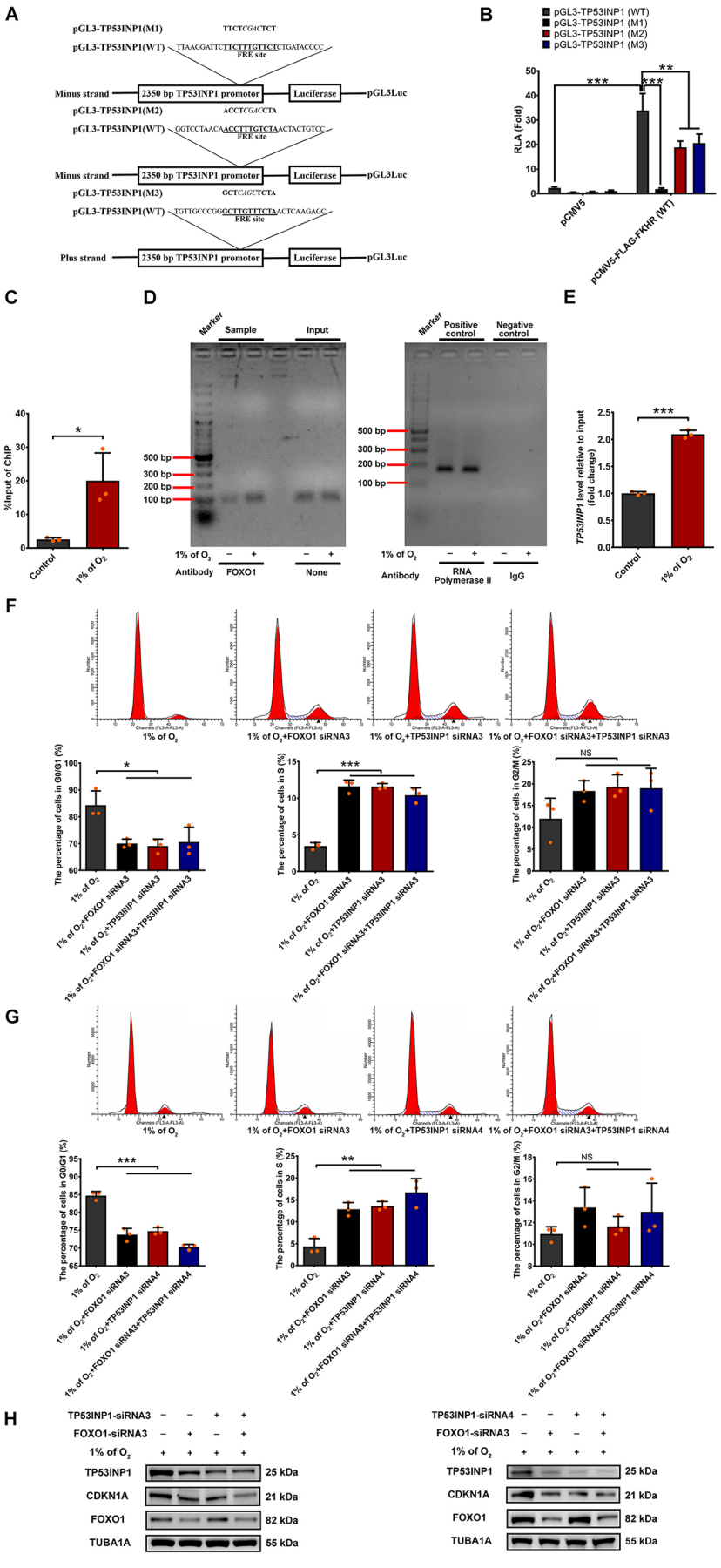

Fig. 4. FOXO1 inhibits the G1- to S-phase progression in hypoxic GCs by activating transcription of *TP53INP1*. (A) A 2072 bp fragment of the *TP53INP1* promoter was amplified by PCR using pig genomic DNA containing three FRE (TGTTTC) motifs and cloned into the pGL3-Basic plasmid as pGL3-TP53INP1(WT). pGL3-TP53INP1 (M1), pGL3-TP53INP1 (M2) and pGL3-TP53INP1 (M3) were individually constructed by introducing mutations (italics) into each of the FRE sites. (B) *TP53INP1* reporter activities in GCs co-transfected with FOXO1 expression vectors and *TP53INP1* promoter constructs for 36 h. The reporter activities were normalized to those of pRL-TK. RLA, relative luciferase activity. (C-E) Binding of FOXO1 to the *TP53INP1* promoter in GCs was detected with ChIP assays following normoxia (20% O_2) or hypoxia (1% O_2) treatment for 12 h. DNA was isolated from the precipitated complexes as a template for qRT-PCR (C). The qRT-PCR products were then analysed on a 2% agarose gel (D) and quantified with densitometry using ImageJ 1.42q software (E). The amount of immunoprecipitated DNA for each ChIP reaction was presented as % input. The *GAPDH* gene promoter immunoprecipitated with RNA polymerase II antibody served as a positive ChIP control. IgG was used as the negative ChIP control. (F,G) GCs transfected with FOXO1 siRNA and/or TP53INP1 siRNAs (siRNA3, siRNA4) for 12 h were exposed to 1% O_2 for 24 h, and then collected for cell cycle analysis using flow cytometry. The cell cycle distribution of GCs was quantified using the ModFit LT 3.2 software. (H) GCs transfected with FOXO1 siRNA and/or TP53INP1 siRNAs for 12 h were grown under hypoxia (1% O_2) for 12 h, and then collected for western blot detection of TP53INP1, CDKN1A and FOXO1 levels in GCs. Data are represented as mean±s.e.m.; n=3. *P<0.05, **P<0.01, ***P<0.001; NS, not significant (P>0.05).

Development (2021) 148, dev199453. doi:10.1242/dev.199453

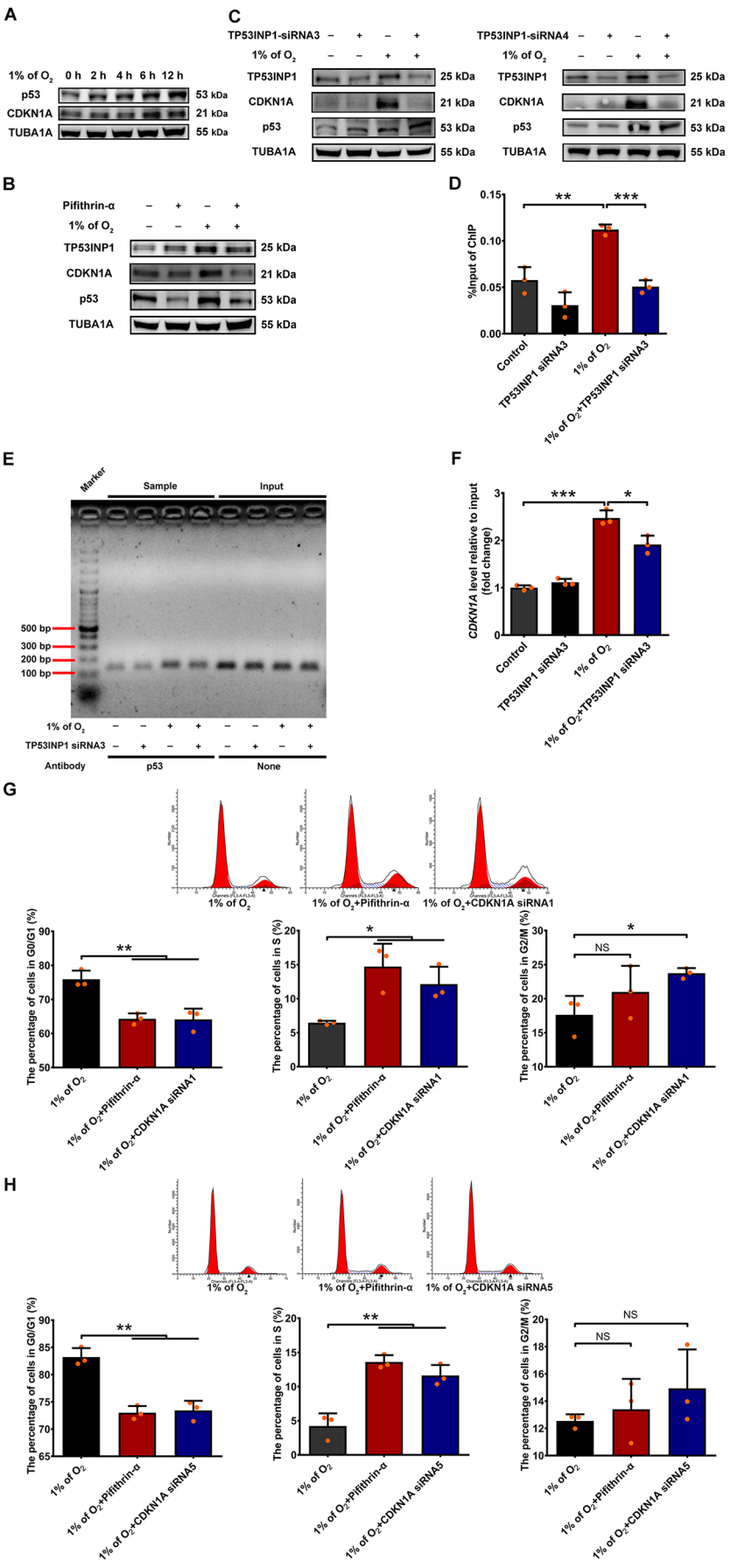

Fig. 5. The effects of TP53INP1 on inhibition of G1-S transition are mediated by activating p53-CDKN1A signalling. (A) GCs exposed to 1% O_2 for 0, 2, 4, 6 or 12 h were retrieved for immunoblotting analysis of p53 and CDKN1A levels. (B-F) GCs were pretreated with the p53 inhibitor pifithrin-α (30 µM) for 2 h (B) or transfected with TP53INP1 siRNA for 12 h (C), and then cultured for an additional 12 h under normoxia (20% O_2) or hypoxia (1% O_2) conditions. The protein levels of TP53INP1, CDKN1A and p53 were determined by western blotting (B,C). The binding of p53 to the *CDKN1A* promoter in GCs was detected with ChIP assays (D-F). DNA was isolated from the precipitated complexes as a template for qRT-PCR (D). The qRT-PCR products were then analysed on a 2% agarose gel (E) and quantified with densitometry using ImageJ 1.42q software (F). (G,H) GCs pretreated with pifithrin-α (30 µM) for 2 h or transfected with CDKN1A siRNAs (siRNA1, siRNA5) for 12 h were then cultured under hypoxia conditions (1% O_2) and, 24 h later, GCs were collected for cell cycle analysis using flow cytometry. The cell cycle distribution of GCs was quantified using the ModFit LT 3.2 software. Data are represented as mean±s.e.m.; n=3. *P<0.05, **P<0.01, ***P<0.001; NS, not significant (P>0.05).

Development (2021) 148, dev199453. doi:10.1242/dev.199453

performed immunofluorescence staining to determine PCNA (reflecting cellular proliferation status) colocalization with TP53INP1 or CDKN1A in GCs within the same follicles (Fig. 6H). The results showed increased expression of both TP53INP1 and CDKN1A in inner layers of GCs, where the levels of PCNA tended to decrease in cells with higher abundance of TP53INP1 or CDKN1A. These data further confirm the relevance of the TP53INP1-CDKN1A axis to GC proliferation retardation at the single-cell level *in vivo*. Taken together, these results suggest that the FOXO1-TP53INP1-p53-CDKN1A axis might mediate hypoxia-induced G0/G1 arrest of ovarian GCs *in vivo*.

DISCUSSION

Various environmental stresses, including oxidative stress, heat stress, cold stress and restraint stress, have been suggested to negatively influence the development of ovarian follicles (Shen et al., 2012). Upon stress stimulation, an arrest or delay of cell cycle progression was observed in immortalized cells of human tumours and other mammalian cell lines (Douglas and Haddad, 2003). Growing evidence implicates hypoxia as one such stress that appears to affect cell cycle activity directly (Douglas and Haddad, 2003). In the ovary, GCs are believed to live in a hypoxic microenvironment inside the follicles (Nishimura and Okuda, 2015). During follicular development, the progressive deficiency in O_2 supply is believed to exacerbate the hypoxic conditions in GCs (Bianco et al., 2005; Redmer and Reynolds, 1996; Suzuki et al., 1998). Our earlier study revealed that chemically mimicked hypoxia caused cell cycle arrest in cultured GCs (Li et al., 2020). However, no definitive evidence exists regarding whether the hypoxia in ovarian follicles exerts any effects on cell cycle regulation of GCs *in vivo*. Here, we show for the first time that hypoxia might represent a principal inhibitory factor in the follicle that blocks the cell cycle transition in ovarian GCs.

The follicular antrum is filled with fluid that absorbs nutrients, hormones and O_2 from the capillary network outside the basement membrane (Brown and Russell, 2014). In particular, the O_2 supplied by blood vessels is transported into GCs by diffusion (Hirshfield, 1991). Predictably, the O_2 content in GCs should be proportional to the diameter of follicles. However, we found that GCs from follicles with similar sizes also showed large variations in hypoxic status as reflected by variations in the accumulation of HIF-1α, a key indicator of cellular hypoxia (Fig. S2). This intriguing phenomenon suggests a possible asynchrony between follicular growth and local angiogenesis. However, the current study discovered that hypoxia is responsible for G0/G1 arrest in ovarian GCs. As the progression from G1 to S phase is a rate-limiting step of cell proliferation (Bertoli et al., 2013), our data indicate that GC proliferation is tightly controlled by the O_2 tension within ovarian follicles. Previous studies have demonstrated a close relationship between GC proliferation and follicular development/atresia (Hirshfield, 1991). Under normal physiological conditions, most follicles become atretic during the 8th or 9th generations of GCs, a time point corresponding to the transition of the growing follicles into mature follicles. At this stage, the GCs have exhausted their proliferative potential, and the follicles do not continue to enlarge. These developmentally arrested follicles will finally be degraded by atresia (Hirshfield, 1991). Therefore, it is conceivable that the asynchronous development of follicles and follicular vasculature interrupts the timely transportation of blood O_2 into the follicular cavity, leading to impaired GC proliferation via cell cycle arrest, which might also elicit selective atresia of certain ovarian follicles.

FOXO1 is a multifunctional transcription factor that plays essential roles in diverse cellular and physiological processes, including cell cycle arrest, proliferation, differentiation, apoptosis, metabolism and aging (Huang and Tindall, 2007). In GCs in particular, FOXO1 has been demonstrated as a key regulator of the stress response (Li et al., 2020; Shen et al., 2018, 2017, 2012, 2014). We previously discovered that a ‘pseudo-hypoxia’ status mimicked by $CoCl_2$ treatment could induce FOXO1-dependent cell cycle arrest in cultured GCs (Li et al., 2020). Here, using high-throughput sequencing technology, we further demonstrated that FOXO1 signalling acts as a crucial mediator of cell cycle inhibition induced by follicular hypoxia in ovarian GCs. Of note, FOXO1 is activated via different molecular mechanisms under ‘real hypoxia’ versus ‘false hypoxia’. Our previous work indicated that PI3K/AKT, a canonical inhibitory pathway of FOXO1, was suppressed during $CoCl_2$ treatment, resulting in the dephosphorylation and nuclear localization of FOXO1 in cultured GCs (Li et al., 2020). By striking contrast, our current data showed that AKT activity was actually increased under ‘real hypoxia’ conditions, but FOXO1 remained in the nuclei of hypoxic GCs. As reported, AKT-mediated phosphorylation of FOXO1 creates binding sites for 14-3-3 chaperone proteins, which promote the nuclear export of FOXO1 (Huang and Tindall, 2007). It thus raised the possibility that hypoxia might block the association between 14-3-3 and FOXO1. Besides AKT, MAPK-related proteins, including SAPK/JNK, p44/42 MAPK and p38 MAPK, are known to regulate FOXO activity upon stress stimuli (Klotz et al., 2015). In this study, we identified JNK as a major upstream activator of FOXO1 in hypoxic GCs. Importantly, JNK enhanced the nuclear translocation of FOXO1 by phosphorylating 14-3-3β/ζ at Ser184/186, which blocked its interaction with FOXO1. Thus, this result might provide an explanation of why AKT failed to influence the cytoplasmic-nuclear shuttling of FOXO1 during ‘real hypoxia’.

TP53INP1 (tumor protein 53-induced nuclear protein 1) is a stress-induced p53 target gene that plays essential roles in cell cycle arrest and p53-mediated apoptosis (Tomasini et al., 2003). Recent studies suggested that FOXO1 activation might increase the expression of *TP53INP1* (Guan et al., 2015; Zhang et al., 2017), but there is little evidence regarding whether this gene is a direct transcription target of FOXO1. Our results showed that FOXO1 stimulated *TP53INP1* expression and activity of its promoter, as well as causing G0/G1 arrest in GCs (Figs S6 and S7). In fact, FOXO1 was found to bind directly to the FRE site within the *TP53INP1* promoter (Fig. 4). Under hypoxic conditions, nuclear transportation of FOXO1 increased its binding with the FRE sequence, which was correlated with upregulated expression of TP53INP1 and increased proportion of cells at G0/G1 (Fig. 3, Fig. S5, Fig. 4). Moreover, we found that *CDKN1A*, a well-described transcriptional target gene of FOXO1 (Huang and Tindall, 2007), was also transcriptionally regulated by TP53INP1. This thus provides evidence for a potential regulation mode of FOXO1-mediated *CDKN1A* transcription in a TP53INP1-dependent manner. Collectively, these data suggest that when GCs are exposed to hypoxia, FOXO1 activates the transcription of *TP53INP1* and its downstream cell cycle inhibitors, such as *CDKN1A*, thereby triggering G0/G1 arrest in GCs.

Because *TP53INP1* expression is regulated by both FOXO1 and p53, we speculate that knockdown of FOXO1 alone cannot completely inhibit the function of TP53INP1. However, we observed that blocking the expression of FOXO1 and TP53INP1 showed similar effects on restoring the passage from G1 to S phase in hypoxic GCs (Fig. 4), implicating FOXO1 as the only upstream

Development (2021) 148, dev199453. doi:10.1242/dev.199453

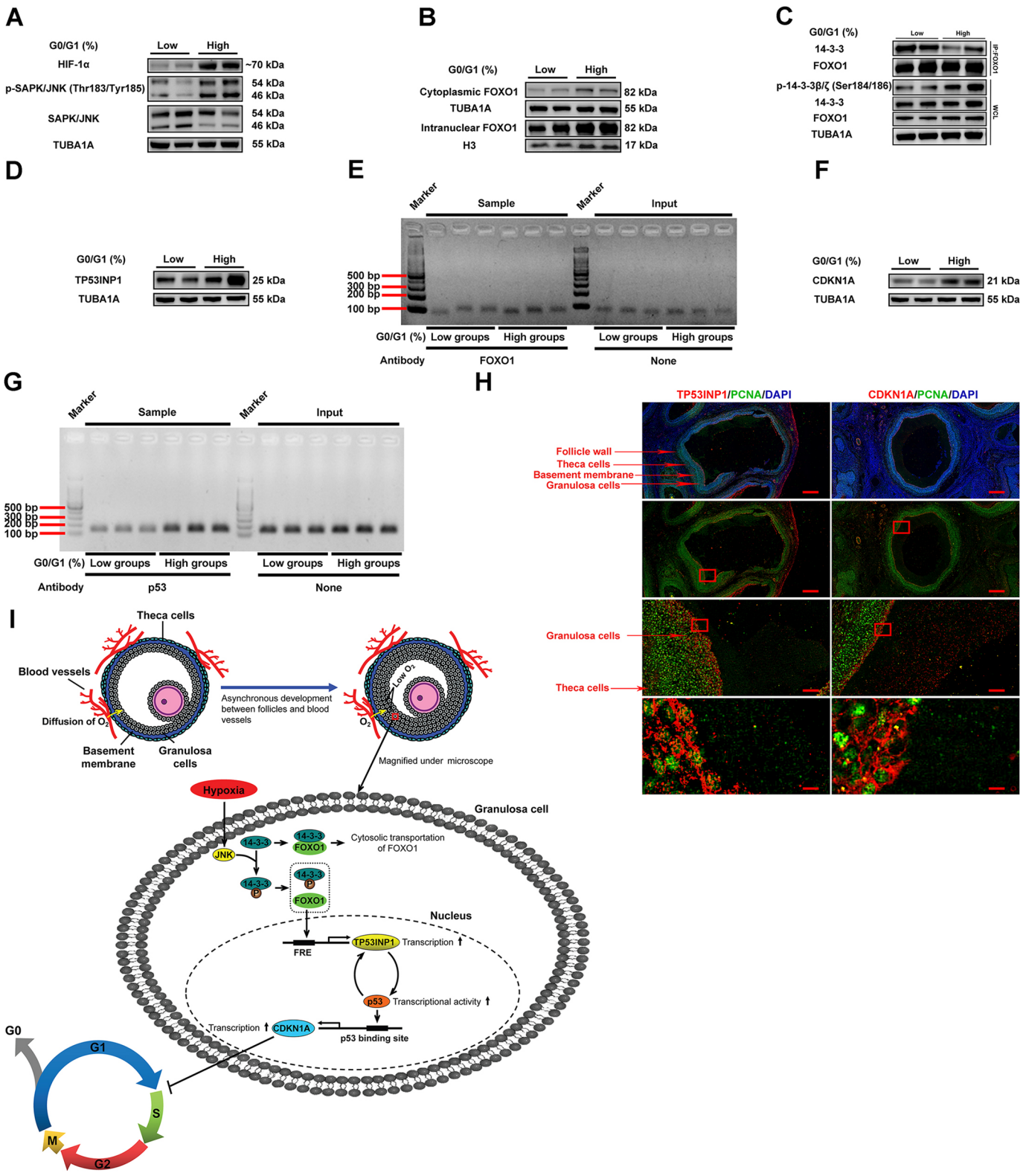

Fig. 6. See next page for legend.

activator of TP53INP1-mediated G0/G1 arrest. Paradoxically, p53 seems to be irrelevant to this process. In fact, we found that there is a bidirectional regulation between TP53INP1 and p53, i.e. p53 promotes the expression of TP53INP1, and TP53INP1 in turn activates p53 transcriptional activity, causing a further increase in TP53INP1 expression levels and p53 transcriptional activity, leading to upregulation of CDKN1A expression and the resultant suppression of G1-S transition (Fig. 5). Further investigations revealed TP53INP1 to be a major activator of p53 transcriptional function in hypoxic GCs (Fig. S10), indicating that p53 is

Development (2021) 148, dev199453. doi:10.1242/dev.199453

Fig. 6. *In vivo* validation of the mechanistic model for cell cycle regulation in ovarian GCs. GCs collected from each of 90 follicles around 4 mm in diameter were labelled with PI for cell cycle analysis. Based on the ratio of cells in G0/G1 phase, GCs were classified into high G0/G1 distribution groups (high groups) and low G0/G1 distribution groups (low groups). (A,B) Western blot showing HIF-1α accumulation, the phosphorylation status of JNK, and intranuclear level of FOXO1 in low and high groups. (C) Immunoprecipitation assay was performed to determine the interaction of 14-3-3 and FOXO1 using the antibodies indicated. WCL, whole cell lysates. (D) The protein levels of TP53INP1 were determined by western blotting. (E) Binding of FOXO1 to the *TP53INP1* promoter in GCs was detected by ChIP. DNA was isolated from the precipitated complexes as a template for qRT-PCR. The qRT-PCR products were then analysed on a 2% agarose gel. (F) The protein levels of CDKN1A were determined by western blotting. (G) ChIP assay was conducted to detect binding of p53 to the *CDKN1A* promoter in low and high groups. (H) Immunofluorescent staining showing localization of PCNA and TP53INP1/CDKN1A protein expression in porcine ovaries. The nuclei were counterstained in DAPI and examined under a laser-scanning confocal microscope. Boxed areas are enlarged in the lower panels. Scale bars: 1000 µm (top four panels); 100 µm (middle two panels); 10 µm (lower two panels). (I) A working model of cell cycle regulation in ovarian GCs during follicular development. In ovarian follicles, the capillary network is confined to the theca cell layer outside the basement membrane, and the O_2 carried by blood vessels is transported into GCs via diffusion. During follicular growth, the asynchronous development between follicles and blood vessels might lead to low O_2 supply (hypoxia) in the inner-layered GCs. In hypoxic GCs, the activation of JNK induces the phosphorylation of 14-3-3, blocking its interaction with FOXO1, resulting in the nuclear translocation of FOXO1, which binds directly to the FRE site within the *TP53INP1* promoter, leading to upregulated expression of TP53INP1. TP53INP1 acts as a major activator of p53 transcriptional function in hypoxic GCs, and p53 in turn promotes the expression of TP53INP1. The positive feedback between TP53INP1 and p53 causes a progressive elevation of TP53INP1 expression levels and p53 transcriptional activity, leading to upregulation of CDKN1A expression and the resultant suppression of G1-S transition.

actually a downstream effector of the FOXO1-TP53INP1 pathway. Therefore, we conclude that activation of the TP53INP1-p53-CDKN1A axis is required for FOXO1-induced G0/G1 arrest in hypoxic GCs.

Conclusions

In summary, this study provides the first evidence suggesting hypoxia as a key stimulus of GC proliferation retardation during follicular development. In addition, we revealed that the activation of FOXO1 by JNK-triggered 14-3-3 phosphorylation is responsible for hypoxia-induced G0/G1 arrest in ovarian GCs. Further investigations identified a novel transcriptional target gene of FOXO1, namely *TP53INP1*, which acts through TP53INP1-p53 positive feedback and p53-CDKN1A signalling to mediate FOXO1-dependent G0/G1 arrest upon hypoxia exposure (Fig. 6I). These findings reveal further insights into the functions of hypoxia in the regulation of folliculogenesis, and provide potential targets for the clinical treatment of reproductive disorders caused by impaired follicular development.

MATERIALS AND METHODS

Reagents and antibodies

SP600125 (S1460) and pifithrin-α (S2929) were purchased from Selleck Chemicals. Antibodies against FOXO1 (2880), p-FOXO1 (9461), TUBA1A (2125), p44/42 MAPK (4695T), p-p44/42 MAPK (4370), Histone H3 (4499), 14-3-3 (8312), p53 (2527), HIF-1α (14179), phospho-SAPK/JNK (Thr183/Tyr185; 4668), SAPK/JNK (9252), AKT (9272), p-AKT (4060) and FLAG (2368) were obtained from Cell Signaling Technology. Antibodies against CDKN1A (10355-1-AP) and p38 MAPK (66234-1-Ig) were obtained from Proteintech. 14-3-3β/ζ (phospho Ser184/186; ABP56527) antibody was purchased from Abbkine. Antibodies against Phospho-p38 MAPK (Thr180/Tyr182; AF4001) and TP53INP1 (DF8731) were obtained from Affinity Biosciences.

Sample collection, cell culture and treatments

Ovaries from mature Duroc-Yorkshire-Landrace sows were collected at a local slaughterhouse and subsequently transferred to the laboratory within 2 h. Ovaries without corpus luteum were selected to isolate morphologically healthy follicles with small forceps. Generally, healthy follicles are rounded with evenly distributed blood vessels; they display pink or yellow in appearance and have a visible cumulus-oocyte complex immersed in clear follicular fluid. After isolation, the follicles were subjected to size measurement, and then individually torn apart to obtain the mural GCs by scraping the follicular wall. GCs were immediately processed for the determination of cell cycle distribution, or restored for RNA-seq, qRT-PCR or immunoblotting analysis. The detailed procedure for the collection of porcine ovarian GCs is depicted as a schematic in Fig. S12. For cell culture, GCs isolated from antral follicles were centrifuged at 1000 ***g*** for 5 min, washed with PBS (Gibco), and then cultured in DMEM/F-12 (1:1) medium (Life Technologies) supplemented with 10% fetal bovine serum (FBS; Sigma-Aldrich) and 100 units/ml penicillin plus 100 µg/ml streptomycin (Gibco) for 2 days. In the control group, cells were maintained at 37°C in a 5% CO_2, 95% air incubator (20% O_2). In the hypoxic group, cells were maintained in a modular incubator chamber flushed with a gas mixture containing 1% O_2, 5% CO_2 and 94% N_2 at 37°C. For drug administration, GCs were treated with the JNK inhibitor SP600125 (10 µM) or the p53 inhibitor pifithrin-α (30 µM) for 2 h, and then incubated 1% O_2 for 12 h or 24 h. For RNA interference, GCs were transfected with FOXO1 siRNA, CDKN1A siRNA, TP53INP1 siRNA or scrambled control siRNA for 12 h, and then exposed to 20% O_2 or 1% O_2 for the indicated time. In some experiments, cells treated with FOXO1 siRNA for 12 h were transfected with the Flag-tagged FOXO1 plasmids or an empty control plasmid, and then cultured with 20% O_2 or 1% O_2 for 12 h or 24 h before they were used for the next assay.

Transcriptome sequencing

GCs collected from antral follicles around 4 mm (4±0.05 mm) in diameter were classified into four groups with two high G0/G1 distribution groups (high groups) and two low G0/G1 distribution groups (low groups), which were then lysed with Trizol reagent (Invitrogen). The cDNA libraries were constructed for each RNA sample using the TruSeq Stranded mRNA Library Prep Kit (Illumina) following the manufacturer's protocol. The libraries were sequenced on an Illumina HiSeq X platform (Illumina) to obtain raw reads. After filtering out low-quality reads and removing the adaptor sequences, we aligned RNA-seq reads to pig genome (Sscrofa11.1, NCBI) using Hisat2 software, and calculated the fragments per kilobase of transcript per million (FPKM) of each gene using Cufflinks. DEGs and corresponding adjusted *P*-values were determined using DEseq2. The biological significance of DEGs was explored by GO term enrichment analysis based on Fisher's exact test and then KEGG pathway enrichment analysis of DEGs was also performed with Fisher's exact test.

Preparation of nuclear and cytosolic protein lysates

Cytosolic and nuclear extracts were prepared according to the manufacturer's instructions of NE-PER Nuclear and Cytoplasmic Extraction Reagents (Thermo Fisher Scientific, 78833). Briefly, GCs were washed twice with ice-cold PBS buffer and centrifuged at 500 ***g*** for 3 min. After the addition of Cytoplasmic Extraction Reagent I, the lysate was incubated on ice for 10 min, and Cytoplasmic Extraction Reagent II was added to the suspension, which was then centrifuged at 16,000 ***g*** at 4°C for 5 min. The supernatant was collected as the cytoplasmic extracts. The insoluble (pellet) fraction was resuspended in Nuclear Extraction Reagent, incubated on ice for 40 min, and then centrifuged at 16,000 ***g*** at 4°C for 10 min. The supernatant was collected as the nuclear extracts. Both nuclear and cytosolic extracts were used for subsequent western blotting experiments.

Immunoblotting assay

Total cell lysate was prepared using ice-cold RIPA Lysis Buffer (Beyotime, P0013B) containing a complete protease inhibitor cocktail (Roche,

Development (2021) 148, dev199453. doi:10.1242/dev.199453

04693132001), and protein concentrations were determined with a bicinchoninic acid (BCA) protein assay kit (Beyotime, P0012). Equal amounts of proteins were separated by electrophoresis on a 4-20% Sure PAGE gel (Genscript) and transferred to PVDF membranes (Millipore) by electroblotting. Nonspecific binding sites were blocked for 1 h with 5% bovine serum albumin (BSA) diluted in Tris-buffered saline with Tween 20 (TBST; Solarbio, Shanghai, China), followed by incubation with the primary antibodies (1:1000) in blocking solution overnight at 4°C. After washing in TBST three times, the membranes were incubated at room temperature for 1 h with an appropriate secondary antibody (1:2000). The immunoblotting signals were then detected under a LAS-4000 luminescent image analyser (Fuji Film Co.) using WesternBright ECL HRP substrate kit (Advansta). The relative expression of each target protein was normalized to that of TUBA1A.

qRT-PCR

Total RNA extracted with TRIZOL reagent (Invitrogen) was reverse transcribed into cDNA using the PrimeScript RT Master Mix (Takara Bio). Real-time PCR was carried out using AceQ qPCR SYBR Green Master Mix (Vazyme) and gene-specific primers (see Table S1 for primer sequences) on the ABI QuantStudio5 system (Applied Biosystems). Specificity of each PCR amplification was verified by melting curve analysis. Data were normalized to the expression of the housekeeping gene *Tuba1a*.

Immunofluorescence

GCs grown on coverslips were subjected to the desired treatments, and fixed with 4% paraformaldehyde (Sigma-Aldrich, P-6148) for 1 h. Cells were washed in PBS (Gibco; 1 mM KH_2PO_4, 155 mM NaCl, 3 mM Na_2HPO_4-$7H_2O$) and then permeabilized with 0.5% Triton X-100 (Sigma-Aldrich, T8787) for 10 min at 4°C. After blocking with 1% BSA (Sigma-Aldrich, A3059) for 1 h at room temperature, the cell climbing sheets were stained with antibody against FOXO1 (2880, Cell Signaling Technology; 1:100) for 1 h at 37°C. Immunoreactivity was detected by incubation with a Rhodamine (TRITC)-conjugated goat anti-rabbit IgG (33109ES60, YEASEN; 1:100) for 1 h at 37°C, and the nuclei were counterstained with DAPI (Sigma-Aldrich, D8417) for 20 min. The slides were then visualized under a Zeiss LSM 710 META confocal microscope (Carl Zeiss). For immunohistological staining, porcine ovaries were fixed in buffered paraformaldehyde (4%), embedded in paraffin, sectioned to approximately 5 µm, and mounted on glass slides. The ovarian sections were deparaffinized in xylene, rehydrated, and retrieved by microwave heating with citrate buffer in 0.05% Tween 20, pH 6.0, for 0.5 h. Endogenous peroxidase activity was eliminated by exposure to 3% H_2O_2 (Sigma-Aldrich, 216763-100 ml) for 10 min. After 1 h of blocking with 1% BSA, sections were incubated with antibodies against TP53INP1 (DF8731, Affinity Biosciences; 1:200), CDKN1A (10355-1-AP, Proteintech; 1:200) or PCNA (Proteintech, 60097-1-Ig; 1:200), and corresponding secondary antibodies [Cy3-AffiniPure goat anti-rabbit IgG (111-165-003, Jackson ImmunoResearch; 1:200) and FITC-AffiniPure goat anti-mouse IgG (115-095-003, Jackson ImmunoResearch; 1:200)], and then mounted with VECTASHIELD Mounting Medium plus DAPI and examined under an LSM 710 META laser-scanning confocal microscope (Carl Zeiss).

Flow cytometry

GCs with desired treatments were digested in 0.25% EDTA-free trypsin (Gibco), rinsed with cold PBS, and fixed with 70% ethanol for 2 h. After twice washing with PBS, cells were centrifuged at 1000 ***g*** for 3 min, and then incubated with propidium iodide (PI)/RNase A staining solution (RNase A:PI=9:1; KeyGEN). The cell cycle distribution was determined using a BD Accuri C6 flow cytometer (Becton Dickinson).

RNA interference

siRNAs specific for *FOXO1*, *TP53INP1*, *CDKN1A* and the scrambled control siRNA were obtained from GenePharma (Shanghai, China). Transfection of siRNAs (see Table S2 for siRNA sequences) was performed with Lipofectamine 3000 reagent (Invitrogen, L3000015) following the manufacturer's instructions.

Immunoprecipitation assay

GCs washed with PBS (Gibco) were lysed on ice with IP lysis buffer (Pierce, 26149) containing protease inhibitor cocktail (Roche, 04693132001). Whole-cell lysates (WCL) were then subjected to immunoprecipitation with anti-FOXO1 (Cell Signaling Technology, 2880). For each immunoprecipitation reaction, we added 5 µl of antibody to 500 µl of cell lysate to reach a final concentration of 20 ng/µl, and the mixture was incubated at 4°C overnight. After addition of 25 µl Protein A/G Magnetic Beads (88802, Thermo Fisher Scientific), the incubation was continued for 1 h at 4°C. The beads were pelleted with magnetic force and the supernatant was discarded. The immunoprecipitates were washed using 1×cell lysis buffer, magnetized again to remove the supernatant, eluted with SDS loading buffer (SunShineBio, Nanjing, China), and then processed for immunoblotting with the indicated antibodies.

ChIP assay

The ChIP assay was performed using a Pierce Agarose ChIP Kit (Thermo Fisher Scientific, 26156) according to the manufacturer's instructions. Briefly, cells were cross-linked with 1% formaldehyde at room temperature for 10 min, and the reaction was stopped by 1× glycine. After washing with cold PBS containing protease inhibitors, cells were lysed in 1 ml SDS lysis buffer (1% SDS, 10 mM EDTA, 50 mM Tris, pH 8.1). Chromatin was then digested with micrococcal nuclease to generate 250-700 bp fragments. For the immunoprecipitation assay, the fragmented chromatin was incubated with anti-FOXO1 (Cell Signaling Technology, 2880), anti-p53 (Cell Signaling Technology, 2527) or rabbit IgG (as control) at 4°C overnight. After degrading proteins in the precipitated complexes with proteinase K, levels of ChIP-purified DNA were quantified with qRT-PCR (see Table S3 for primer sequences). The amount of immunoprecipitated DNA for each ChIP reaction was calculated using the Percent Input Method and was presented as percentage input.

Luciferase reporter gene assay

The *TP53INP1* promoter was amplified with PCR from pig genomic DNA (2072 bp, 5′-UTR of *TP53INP1*), cloned into the pGL3-Basic plasmid (Promega) at the KpnI and XhoI (Takara Bio) sites and named pGL3-TP53INP1(WT) (see Table S4 for primer sequences). By searching the JASPAR database (http://jaspar.genereg.net/), we identified three FRE (TGTTTC) motifs within the *TP53INP1* promoter region. Using a Mut Express II Fast Mutagenesis Kit (Vazyme, China), pGL3-TP53INP1 (M1), pGL3-TP53INP1 (M2) and pGL3-TP53INP1 (M3) were individually constructed by introducing mutations into each of these FRE sites. Transfection was performed with Lipofectamine 3000 (Invitrogen). Three plasmids were co-transfected in each treatment: (1) 1.6 µg expression vector pCMV5-FLAG-FKHR (WT); (2) 1.6 µg reporter construct pGL3-TP53INP1(WT), pGL3-TP53INP1(M1), pGL3-TP53INP1(M2) or pGL3-TP53INP1(M3); and (3) 32 ng control reporter pRL-TK (Promega). Luciferase activities were measured 36 h post-transfection using the Dual-luciferase Reporter Assay System (Promega) and Modulus Microplate Luminometer (Turner BioSystems) according to the manufacturers' protocols. Data are presented as firefly luciferase reporter values normalized to *Renilla* values.

Statistical analysis

Statistical analysis was performed using the SPSS software version 20.0 (SPSS). All experiments were repeated at least three times, and the data are presented as mean±s.e.m. Pairwise comparisons were assessed by the Student's *t*-test, and *P*-values <0.05 were considered to be statistically significant.

Competing interests

The authors declare no competing or financial interests.

Author contributions

Conceptualization: C.L., M.S., H.L.; Methodology: C.L., J.-Q.Z., J.T., M.S.; Software: C.L., M.S.; Validation: C.L., M.S.; Formal analysis: C.L., M.S.; Investigation: C.L., Z.L., G.W., Z.Z., X.L., M.S.; Resources: C.L., M.S.; Data curation: C.L., M.S.; Writing - original draft: C.L., M.S.; Writing - review & editing: C.L., M.S.;

Visualization: C.L., M.S.; Supervision: M.S., H.L.; Project administration: M.S., H.L.; Funding acquisition: C.L., M.S., H.L.

Funding
This work was supported by The National Natural Science Foundation of China (31972564; 31972571; 31630072; 31601939), a project funded by the Priority Academic Program Development of Jiangsu Higher Education Institutions (DKQB201903), the Postgraduate Research & Practice Innovation Program of Jiangsu Province funded by the Jiangsu Provincial Department of Education (KYCX20_0602), and the National Major Project for Breeding of Transgenic Pigs funded by the Ministry of Agriculture and Rural Affairs of the People's Republic of China (2016ZX08006001-003).

Data availability
RNA-seq data have been deposited in the Gene Expression Omnibus database under accession number GSE175641.

Peer review history
The peer review history is available online at https://journals.biologists.com/dev/article-lookup/doi/10.1242/dev.199453

References
Bertoli, C., Skotheim, J. M. and de Bruin, R. A. (2013). Control of cell cycle transcription during G1 and S phases. *Nat. Rev. Mol. Cell Biol.* **14**, 518-528. doi:10.1038/nrm3629
Bianco, F., Basini, G., Santini, S. and Grasselli, F. (2005). Angiogenic activity of swine granulosa cells: effects of hypoxia and the role of VEGF. *Vet. Res. Commun.* **29** Suppl. 2, 157-159. doi:10.1007/s11259-005-0031-3
Brown, H. M. and Russell, D. L. (2014). Blood and lymphatic vasculature in the ovary: development, function and disease. *Hum. Reprod. Update* **20**, 29-39. doi:10.1093/humupd/dmt049
Douglas, R. M. and Haddad, G. G. (2003). Genetic models in applied physiology: invited review: effect of oxygen deprivation on cell cycle activity: a profile of delay and arrest. *J. Appl. Physiol. (1985)* **94**, 2068-2083. doi:10.1152/japplphysiol.01029.2002
Gardner, L. B., Li, Q., Park, M. S., Flanagan, W. M., Semenza, G. L. and Dang, C. V. (2001). Hypoxia inhibits G1/S transition through regulation of p27 expression. *J. Biol. Chem.* **276**, 7919-7926. doi:10.1074/jbc.M010189200
Gougeon, A. (1996). Regulation of ovarian follicular development in primates: facts and hypotheses. *Endocr. Rev.* **17**, 121-155. doi:10.1210/edrv-17-2-121
Guan, H., Tan, P., Xie, L., Mi, B., Fang, Z., Li, J., Yue, J., Liao, H. and Li, F. (2015). FOXO1 inhibits osteosarcoma oncogenesis via Wnt/β-catenin pathway suppression. *Oncogenesis* **4**, e166. doi:10.1038/oncsis.2015.25
Harper, J. W., Elledge, S. J., Keyomarsi, K., Dynlacht, B., Tsai, L. H., Zhang, P., Dobrowolski, S., Bai, C., Connell-Crowley, L., Swindell, E. et al. (1995). Inhibition of cyclin-dependent kinases by p21. *Mol. Biol. Cell* **6**, 387-400. doi:10.1091/mbc.6.4.387
Hirshfield, A. N. (1991). Development of follicles in the mammalian ovary. *Int. Rev. Cytol.* **124**, 43-101. doi:10.1016/S0074-7696(08)61524-7
Huang, H. and Tindall, D. J. (2007). Dynamic FoxO transcription factors. *J. Cell Sci.* **120**, 2479-2487. doi:10.1242/jcs.001222
Klotz, L. O., Sánchez-Ramos, C., Prieto-Arroyo, I., Urbánek, P., Steinbrenner, H. and Monsalve, M. (2015). Redox regulation of FoxO transcription factors. *Redox Biol.* **6**, 51-72. doi:10.1016/j.redox.2015.06.019
Li, Y., Jenkins, C. W., Nichols, M. A. and Xiong, Y. (1994). Cell cycle expression and p53 regulation of the cyclin-dependent kinase inhibitor p21. *Oncogene* **9**, 2261-2268.
Li, C., Liu, Z., Zhou, J., Meng, X., Liu, S., Li, W., Zhang, X., Yao, W., Dong, C., Cao, Y. et al. (2020). Insulin-like growth factor-I prevents hypoxia-inducible factor-1 alpha-dependent G1/S arrest by activating cyclin E/cyclin-dependent kinase2 via the phoshatidylinositol-3 kinase/AKT/forkhead box O1/Cdkn1b pathway in porcine granulosa cellsdagger. *Biol. Reprod.* **102**, 116-132.
Munakata, Y., Kawahara-Miki, R., Shiratsuki, S., Tasaki, H., Itami, N., Shirasuna, K., Kuwayama, T. and Iwata, H. (2016). Gene expression patterns in granulosa cells and oocytes at various stages of follicle development as well as in in vitro grown oocyte-and-granulosa cell complexes. *J. Reprod. Dev.* **62**, 359-366. doi:10.1262/jrd.2016-022
Nishimura, R. and Okuda, K. (2015). Multiple roles of hypoxia in ovarian function: roles of hypoxia-inducible factor-related and -unrelated signals during the luteal phase. *Reprod. Fertil. Dev.* doi:10.1071/RD15010
Ortmann, B., Druker, J. and Rocha, S. (2014). Cell cycle progression in response to oxygen levels. *Cell. Mol. Life Sci.* **71**, 3569-3582. doi:10.1007/s00018-014-1645-9
Ramaswamy, S., Nakamura, N., Sansal, I., Bergeron, L. and Sellers, W. R. (2002). A novel mechanism of gene regulation and tumor suppression by the transcription factor FKHR. *Cancer Cell* **2**, 81-91. doi:10.1016/S1535-6108(02)00086-7
Redmer, D. A. and Reynolds, L. P. (1996). Angiogenesis in the ovary. *Rev. Reprod.* **1**, 182-192. doi:10.1530/ror.0.0010182
Robker, R. L. and Richards, J. S. (1998). Hormone-induced proliferation and differentiation of granulosa cells: a coordinated balance of the cell cycle regulators cyclin D2 and p27Kip1. *Mol. Endocrinol.* **12**, 924-940. doi:10.1210/mend.12.7.0138
Shen, M., Cao, Y., Jiang, Y., Wei, Y. and Liu, H. (2018). Melatonin protects mouse granulosa cells against oxidative damage by inhibiting FOXO1-mediated autophagy: implication of an antioxidation-independent mechanism. *Redox Biol.* **18**, 138-157. doi:10.1016/j.redox.2018.07.004
Shen, M., Jiang, Y., Guan, Z., Cao, Y., Li, L., Liu, H. and Sun, S. C. (2017). Protective mechanism of FSH against oxidative damage in mouse ovarian granulosa cells by repressing autophagy. *Autophagy* **13**, 1364-1385. doi:10.1080/15548627.2017.1327941
Shen, M., Lin, F., Zhang, J., Tang, Y., Chen, W. K. and Liu, H. (2012). Involvement of the up-regulated FoxO1 expression in follicular granulosa cell apoptosis induced by oxidative stress. *J. Biol. Chem.* **287**, 25727-25740. doi:10.1074/jbc.M112.349902
Shen, M., Liu, Z., Li, B., Teng, Y., Zhang, J., Tang, Y., Sun, S. C. and Liu, H. (2014). Involvement of FoxO1 in the effects of follicle-stimulating hormone on inhibition of apoptosis in mouse granulosa cells. *Cell Death Dis.* **5**, e1475. doi:10.1038/cddis.2014.400
Sunayama, J., Tsuruta, F., Masuyama, N. and Gotoh, Y. (2005). JNK antagonizes Akt-mediated survival signals by phosphorylating 14-3-3. *J. Cell Biol.* **170**, 295-304. doi:10.1083/jcb.200409117
Suzuki, T., Sasano, H., Takaya, R., Fukaya, T., Yajima, A. and Nagura, H. (1998). Cyclic changes of vasculature and vascular phenotypes in normal human ovaries. *Hum. Reprod.* **13**, 953-959. doi:10.1093/humrep/13.4.953
Tomasini, R., Samir, A. A., Carrier, A., Isnardon, D., Cecchinelli, B., Soddu, S., Malissen, B., Dagorn, J. C., Iovanna, J. L. and Dusetti, N. J. (2003). TP53INP1s and homeodomain-interacting protein kinase-2 (HIPK2) are partners in regulating p53 activity. *J. Biol. Chem.* **278**, 37722-37729. doi:10.1074/jbc.M301979200
Vanderhyden, B. C., Telfer, E. E. and Eppig, J. J. (1992). Mouse oocytes promote proliferation of granulosa cells from preantral and antral follicles in vitro. *Biol. Reprod.* **46**, 1196-1204. doi:10.1095/biolreprod46.6.1196
Zhang, W., Duan, N., Song, T., Li, Z., Zhang, C. and Chen, X. (2017). The emerging roles of Forkhead box (FOX) proteins in osteosarcoma. *J. Cancer* **8**, 1619-1628. doi:10.7150/jca.18778
Zhang, Y., Yan, Z., Qin, Q., Nisenblat, V., Chang, H. M., Yu, Y., Wang, T., Lu, C., Yang, M., Yang, S. et al. (2018). Transcriptome landscape of human folliculogenesis reveals oocyte and granulosa cell interactions. *Mol. Cell* **72**, 1021-1034.e1024. doi:10.1016/j.molcel.2018.10.029